RSC Advances

PAPER

View Article Online
View Journal | View Issue

Cite this: *RSC Adv.*, 2024, **14**, 13972

Molecular dynamics simulation of the initial stage induction of alkali-activated aluminosilicate minerals

Feng Guo,[b] Jizhou Chen,[c] Qingyin Tang,[a] Mengqi Sun,[a] Haibao Feng,[de] Hailiang Gao,[f] Mengmeng Li*[a] and Shuang Lu[g]

With the increasing global concern over carbon emissions, geopolymers have garnered significant attention due to their energy-saving, waste utilization, and eco-friendly advantages. Metakaolin and slag, as aluminum-containing mineral materials in geopolymer production, have been widely studied and applied. Previous research has mainly focused on performance design and theoretical development, while the underlying mechanisms at the microscopic level remain unclear. In this study, we employed molecular dynamics simulations to investigate the microscale reaction behavior of geopolymers, exploring the induction process and structural evolution during the initial stages, and revealing the similarities and differences under alkali activation for different materials. Our findings indicate that the alkali activation process can be divided into two stages: mineral crystal deconstruction and oligomer polymerization. The role of NaOH differs between low-calcium and high-calcium systems, where in the low-calcium system, Na^+ substitutes Ca^{2+} due to Ca^{2+} deficiency, participating in the formation of the network framework. Moreover, the high-calcium system exhibits a faster formation of the gel phase during alkali activation compared to the low-calcium system. This study provides valuable insights into the research and application of geopolymers.

Received 1st February 2024
Accepted 19th April 2024

DOI: 10.1039/d4ra00822g

rsc.li/rsc-advances

1 Introduction

In the field of engineering and construction, geopolymer cementitious materials have received widespread attention. Geopolymers are green, low-energy, and sustainable building materials, and their development and application can be closely linked to global carbon emissions,[1] thereby reducing carbon emissions and promoting resource recycling.[2] With the introduction of "dual-carbon" targets,[3] these materials are favored because of their low carbon footprint, high strength, high durability, and a wide choice of raw materials.

In recent years, with the research and application of geopolymers, raw material composites are often used in practical engineering to promote the utilization of solid wastes and improve their strength and performance.[2] The study of geopolymer cementitious materials involves many aspects such as material composition, preparation process, performance, *etc.* However, the different and complex raw materials, lead to the difficulty of predicting the reaction products of the composite system, so the study of the microstructure of the reaction products is particularly important. Raw material composition affects reaction products. As an important aluminum-containing mineral material, metakaolin (MK) and slag show great potential in the fields of catalysis, adsorption, ion exchange, and nanomaterials. Mostly, geopolymers are now prepared by replacing cement with metakaolin or slag. As a calcium-rich raw material, the reaction product of slag is usually CASH,[4–6] while the reaction product of silica- and aluminium-rich MK is usually NASH[7–9] after alkali activation, *etc.* The difference in the reaction products leads to the difference in the strength and properties of geopolymers.

Geopolymers have excellent properties. To enhance the practical application of slag-based geopolymers, Albitar *et al.*[10] conducted a study on the load-bearing aspects and found that they exhibit structural properties similar to Portland cement (PC). Gómez-Casero *et al.*[11] conducted a study on metakaolin-based geopolymers and found that the metakaolin-based geopolymers exhibit excellent compressive strength and thermal insulation performance, with lower thermal conductivity compared to PC. Catauro *et al.*[12] investigated the structural stability of metakaolin-based geopolymers with and without the

[a]*Department of Civil Engineering, Qingdao University of Technology, Qingdao 266033, China. E-mail: limengmeng7@126.com*
[b]*Beijing Jingtou Transportation Development Co., Ltd., Beijing 102629, China*
[c]*Qingdao Municipal Group Co., Ltd., Qingdao 266003, China*
[d]*CCCC First Harbor Engineering Co., Ltd., Tianjin 300461, China*
[e]*The Second Engineering Co., Ltd., of CCCC First Harbor Engineering Co., Ltd., Qingdao 266071, China*
[f]*Qingdao Municipal Engineering Design Research Institute Co., Ltd., Qingdao 266061, China*
[g]*School of Civil Engineering, Harbin Institute of Technology, Harbin 150090, China*

addition of fly ash and observed that the composite materials exhibited excellent durability and comparable compressive strength to PC. Siyal *et al.*[13] compiled the research on the adsorption of heavy metals and dyes by geopolymers and found that geopolymers possess favorable surface properties and microstructure that enable highly efficient adsorption of heavy metal ions and dyes, exhibiting spontaneous adsorption behavior. Geopolymers prepared using materials such as slag and fly ash by Marathe *et al.*[14] demonstrate excellent performance under normal road working conditions. These practical studies and applications can validate their performance and feasibility in real-world engineering environments.

Much of the current experimental research has focussed on the design of mixing ratios for geopolymers and has provided a great deal of useful information for the theoretical development of geopolymers. Jaya *et al.*[15] investigated the effect of metakaolin content on the properties of geopolymers and found that adjusting the ratio of metakaolin to alkali activator gave the highest compressive strength and that the ratio of alkali activator was the determining factor in the strength. Wang *et al.*[16] investigated geopolymers with five different metakaolin content ranging from 0% to 100%, activated using a mixed alkaline activator solution containing NaOH. It was found that as the substitution rate of metakaolin increased, the microstructure of geopolymers became more porous, leading to a greater degradation of relevant properties. Ratio and content affect the structure and properties of geopolymers. Jamil *et al.*[17] conducted experiments on geopolymer composites containing both kaolin and slag to investigate the influence of sintering parameters on their mechanical properties. They found that different sintering parameters led to alterations in the microstructure of geopolymer composites. Subsequently, they examined the impact of slag composition on the phase transition of geopolymers and discovered that the presence of oxides of silicon, aluminum, calcium, and magnesium in the slag accelerated the phase transition process.[18] After accumulating a large amount of research data, researchers began to focus on microstructures and reaction processes to clarify the reaction mechanism of geopolymers.

However, there is considerably less available information regarding the induction reaction process of geopolymer concrete at the microstructural level. Xia *et al.*[19] conducted a study on the early structural evolution process of geopolymers using proton nuclear magnetic resonance (H-1 NMR) and divided it into four stages: induction, acceleration, deceleration, and stabilization. Building upon this, further scholars have explored the microreactive process of geopolymers. Liu *et al.*[20] investigated the effect of adding high-alkali red mud while using NaOH as an alkaline activator and found that increasing the alkalinity facilitated the activation of minerals, resulting in shorter induction periods and higher hydration rates. Subsequently, they further studied the influence of alkali content and observed that a higher concentration of NaOH accelerated the hydration process, reducing the induction time.[21] However, excessive alkali content led to the accumulation of microstructural defects and a subsequent decrease in specimen strength. Ma *et al.*[22] investigated the influence of Na_2SO_4 content on the microstructure of geopolymer using Na_2SO_4 as an activator. They found that Na_2SO_4 content caused a relative prolongation of the induction period and resulted in volumetric expansion during the initial stages. Gu *et al.*[23] researched FA-GBFS geopolymer and found that the synergistic effect between mineral polycondensation reactions and calcium silicate hydration reactions determines the mechanical and magnetic properties of this type of geopolymer. Although these studies exploring the microreaction mechanism of geopolymers have provided us with a large amount of theoretical data, the experiments are difficult to provide more detailed reaction information at the nanometre level due to the limitation of equipment conditions and the microreaction mechanism is still unclear.

Molecular dynamics (MD) simulation is a crucial research tool. It not only validates experimental phenomena but also unveils the dynamic behavior of materials by simulating interactions between atoms or molecules. Many scholars have investigated geopolymers using MD simulation methods to explore the mechanism of action at the nano level, which is widely recognized in the industry. Tian *et al.*[24] employed the MD method to investigate the interfacial behavior of geopolymers and discovered that hydrogen bonding affects the interfacial adsorption of water molecules. Furthermore, the formation of complex ion clusters between metal ions and water molecules enhances interfacial bonding, resulting in improved tensile and shear strength. Wang *et al.*[25] conducted MD simulations to investigate the influence of Na^+ and H_2O on the microstructure of geopolymers, and found that a higher concentration of both species leads to a more stable structure. Subsequently, Wang *et al.*[26] conducted MD simulations on the adsorption of heavy metal ions by geopolymers and observed that the composition of the reaction products directly affects the adsorption of radioactive nuclides, with a lower Al/Si ratio corresponding to a stronger adsorption capacity. Tang *et al.*[27] investigated the anti-erosion mechanism of NASH, and they found that in a salt solution, the adsorption sites inside NASH were able to trap external Na^+ ions, which retarded the decomposition or fracture of the three-dimensional network skeleton, which resulted in good resistance to sulfate erosion. These studies have focused on the interactions of geopolymers with other substances, but there are still fewer studies on the reaction processes of alkali-activated geopolymers. Yin *et al.*[28] proposed that the alkali activation process of fly ash consists of four main stages: dissolution stage, depolymerization stage, condensation stage, and diffusion stage, which ultimately produces a zeolite-like three-dimensional reticulated NASH gel structure with Q4 as the structural unit. Hou *et al.*[29] studied the alkali-activated processes of metakaolin and found that the silicates dissolved while the more stable aluminates did not. Luo *et al.*[30] also studied the alkali-activated processes of metakaolin and found that aluminum, which is more active during the induction process, not only preferentially participates in the reaction, but also balances the structural charge. These molecular modeling studies are all about low-calcium-geopolymers. However, geopolymer cementitious materials are divided into two main groups: low-calcium (NASH) and high-calcium (CASH), which have different hydration processes and microstructural

evolutions due to the differences in Ca^{2+} content and the high reactivity of Ca^{2+} with NaOH solutions. Therefore, there is a lack of research on the microreaction process of alkali-activated high-calcium-geopolymers.

Under alkali activation, silicate and aluminate oligomers obtained from minerals such as metakaolin and slag, along with water and various ions, serve as important precursor species for the formation of NASH (sodium aluminate silicate hydrate) and CASH (calcium aluminate silicate hydrate). Therefore, gaining a deeper understanding of the early-stage behavior of alkali-activated metakaolin and slag in the formation of oligomeric precursors can provide valuable insights and guidance for the preparation, modification, and application of geopolymers. Despite the extensive research focused on the physicochemical properties of alkali-activated metakaolin and slag, the understanding of the molecular dynamical behavior induced during their initial stages remains limited. Instead, in this study, we use molecular dynamics simulations to explore the initial phase behavior of metakaolin and slag under alkali activation, to analyze the differences in the role of NaOH in the low and high-calcium systems, and to reveal the similarities and differences between the different materials under alkali activation conditions. We will focus on intermolecular interactions, ionic migration, and structural evolution to explore the microscopic reaction mechanisms and reveal the microscopic properties of these two materials under alkali activation conditions, to contribute to the application of these materials and research in related fields.

2 Simulation details

2.1 Model construction

To study the initial induced behavior of the dissociation of metakaolin and slag into aluminosilicate oligomeric precursors in alkaline environments, we constructed crystal models of metakaolin and slag. Metakaolin is synthesized by calcining kaolin. We have employed a combined approach of total scattering techniques, coordination distribution functions, and density functional models, as proposed by White *et al.*,[31] to construct a molecular dynamics model for metakaolin. As shown in Fig. 1(a), the initial cell parameters of the selected kaolinite are a = 5.1535 Å, b = 8.9419 Å, c = 7.3906 Å, α = 91.926°, β = 105.046° and γ = 89.797°. First, the model of metakaolin was transformed into a form resembling a nearly square crystal unit cell and subjected to a 2 × 6 × 6 supercell treatment. Subsequently, 87.5% of the hydrogen atoms and 19.5% of the oxygen atoms were removed from the supercell system. This dehydroxylation method was based on relevant data obtained from thermogravimetric analysis of kaolinite heated to 750 °C.[32,33] All internal hydrogen atoms were removed, and the remaining hydroxyl groups were used to isolate the inner surface of the aluminum silicate layers. Relevant references have demonstrated that this structure does not collapse along the *C*-axis.[32,34] Calcium feldspar is a significant component of slag. A calcium feldspar unit cell was selected as the activation system for simulating the slag. The crystallographic parameters of the unit cell are a = 8.173 Å, b = 12.869 Å, c = 14.165 Å, α = 93.113°, β = 115.913°, and γ = 89.797°. The initial unit cell was first transformed into a form resembling an orthogonal unit cell and then subjected to a supercell treatment of 1 × 5 × 3. The resulting structure is shown in Fig. 1(b).

Metakaolin and slag, as crucial precursors, react with alkaline solutions to respectively produce NASH and CASH. Consequently, it is imperative to establish an interface model between the solution and the precursors. Cutting the (0 0 1) plane of metakaolin and slag is performed to construct precursor surfaces, thereby exposing Al–O, Si–O, and Al–OH groups on the surface. The constructed crystal model was then put into NaOH solution with 6% solubility for alkali activation as shown in Fig. 2. Granizo *et al.*[35] investigated the effect of alkali concentration on metakaolin-based geopolymers and found that the best activation effect with a significant increase in strength was achieved when the molar concentration of alkali was within the range of 4 to 8 moles. Dai *et al.*[36] investigated the effect of NaOH concentration on the rheological properties and

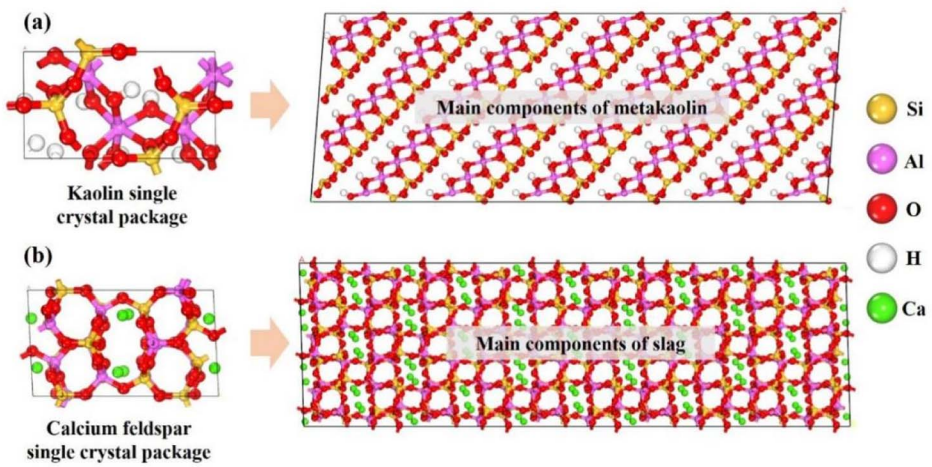

Fig. 1 (a) Construction of a metakaolin cell from a kaolinite cell; (b) construction of a slag cell from a calcite feldspar cell; on the right-hand side of the picture are the types of atoms represented by the individual spheres.

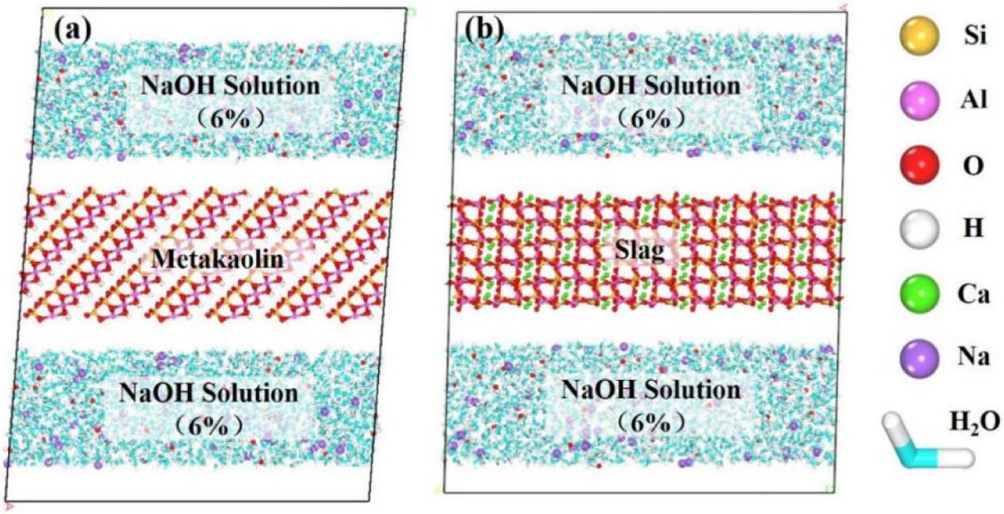

Fig. 2 The initial simulation system of alkali-activated geopolymers.

early-stage reaction process of alkali-activated finely ground granulated blast furnace slag (GGBFS). They found that as the NaOH concentration increased, the initial setting time of AAS (alkali-activated slag) mortar decreased, and the yield stress and apparent viscosity increased. Therefore, a NaOH solution concentration of 6% was chosen for the simulations.

2.2 Force field selection

The chemical reactions involved in this study were simulated using ReaxFF. This reactive force field is capable of modeling the breaking of existing bonds and the formation of new bonds, with potential energy calculations including electron transfer and recombination between atoms:

$$E_{\text{Total}} = E_{\text{Bond}} + E_{\text{over}} + E_{\text{under}} + E_{\text{val}} + E_{\text{pen}} + E_{\text{tors}} + E_{\text{conj}} + E_{\text{vdWaals}} + E_{\text{Coulomb}}$$

where E_{Bond} is the bond energy, E_{over} and E_{under} represent the energy correction terms for over-coordination and under-coordination, respectively, E_{val} represents the valence angle energy, E_{pen} represents the penalty energy, E_{tors} represents the torsional energy, E_{conj} is the conjugation effect of the molecule, E_{vdWaals} is the non-bonding van der Waals force, and E_{Coulomb} is the non-bonding Coulomb force. The ReaxFF parameters for each atom can be obtained from the information developed and published by van Duin *et al.*[37] in the reference. To ensure the optimal applicability of the parameters during the simulation process, they have been obtained through high-precision fitting. The accuracy of these parameters has been validated in practical applications, being widely utilized in the micro-structural evolution of CSH,[38,39] reaction hydrolysis processes,[40] as well as the microbehavior of geopolymers.[41]

2.3 Alkali activation simulation process

We started the simulation process of the alkali-activated geopolymer system on the LAMMPS[42] software by first applying periodic boundaries in the *X*, *Y*, and *Z* directions of the model to ensure a constant number of particles in the simulated system. The time step for the entire simulation process was set as 0.25 fs. Subsequently, a relaxation period of 500 ps was conducted under the NPT ensemble to maintain a constant system temperature of 300 K. This sufficiently long relaxation process allows the system to contract to a zero-pressure state, ensuring the convergence of potential energy and volume in the simulated model. Next, the system was uniformly heated from 300 K to 1800 K at a rate of 7.5 K ps^{-1}, followed by a constant temperature equilibration at 1800 K for 500 ps. This allows the atoms to remain in an active, high-speed motion state, promoting the alkali activation process of the mineral raw materials, accelerating the formation of oligomers, and reducing the simulation time of the activation process. At this temperature, the mineral raw materials have been sufficiently activated. Subsequently, the system was annealed at the same rate from 1800 K to 300 K for equilibration. Finally, to obtain structurally stable and reasonable simulation results, the system underwent a relaxation process of 300 ps at a constant temperature of 300 K. The entire simulation process was carried out under the NPT ensemble. The entire simulation process was conducted on a 120-core workstation, with each model utilizing 60 cores for computation. The simulation process took approximately two weeks to complete.

3 Results and discussion

3.1 Mineral leaching phenomenon

Fig. 3(a) and (b) shows the effect of being excited in a 6% NaOH solution environment for metakaolin and slag, respectively. As shown in Fig. 3(a), we observed that metakaolin has transformed from a layered crystal structure to a disordered amorphous state. At the interface region in contact with the NaOH solution, some H_2O molecules, OH^- ions, and Na^+ ions have infiltrated into the internal structure of the matrix.

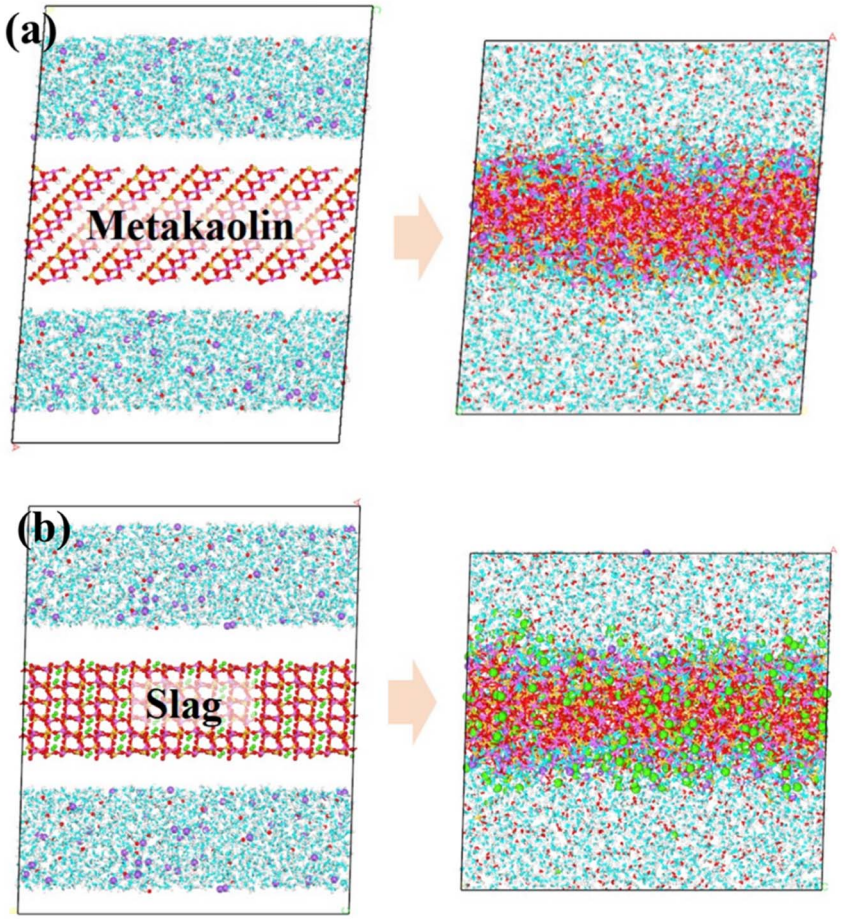

Fig. 3 (a) Alkali activation effect of metakaolin. (b) Alkali activation effect of slag.

Simultaneously, the dissociated crystal structure exists in the solution as free silicate monomers. This indicates that metakaolin has undergone dissociation, with a portion of the aluminosilicate framework being eroded and dissolved by the NaOH solution, leading to the formation of oligomeric structures. In Fig. 3(b), the interconnected structure of the calcium feldspar has also transformed into an unordered amorphous structure. At the interface region, some water molecules and OH^- ions have infiltrated into the matrix structure, while Na^+ ions only adsorb on the surface of the matrix without embedding into deeper positions. Simultaneously, a large amount of Ca^{2+} ions undergo dissociation, and a small amount of silicate dissociates into $Si(OH)_4$, existing as oligomers in the solution. By comparing these two figures, it can be observed that there are certain differences in the dissolution behavior of the low-calcium and high-calcium types of geopolymer precursors.

To quantitatively analyze the dissolution of various atom types after NaOH activation, density distribution plots were generated as shown in Fig. 4. The central blue region represents the mineral crystals, while the red regions on both sides represent the NaOH solution. After the heating and annealing process, there were changes in the distribution of atoms. Fig. 4(a) displays the atomic density distribution of metakaolin after activation, clearly exhibiting the diffusion of some oxygen atoms (O-MK) from the crystal structure into the solution, consistent with the previous analysis. Combining Fig. 3 and 4, and referring to relevant ref. 43, it can be observed that the MK matrix underwent partial decomposition. In addition, oxygen atoms (O_W) and OH^- ions infiltrated partially from the solution into the matrix, while Na^+ ions fully penetrated the matrix from the solution. This indicates that under the activation of the NaOH solution, the original structure of MK is disrupted and a new structure is formed. According to the relevant ref. 43, this newly formed phase is identified as the NASH gel phase. Na^+ serves as an important constituent of the NASH gel phase, uniformly distributed in the interstitial spaces of the aluminosilicate framework. It plays a role in maintaining charge balance in the system. Therefore, the entry of Na^+ into the matrix provides a crucial ion component for the formation of NASH. Fig. 4(b) displays the atomic density distribution of the activated slag, showing similar characteristics to the alkali-activated metakaolin. It is evident that some oxygen atoms (O-slag) diffuse into the solution from the crystal structure, and a portion of Ca^{2+} leaches out from the ordered crystal lattice into the solution, indicating the disruption of the slag structure. Additionally, the behavior of oxygen atoms (O_W) and OH^- ions in the solution is similar to that observed in Fig. 4(a), with partial infiltration into the structure. These behaviors lead to

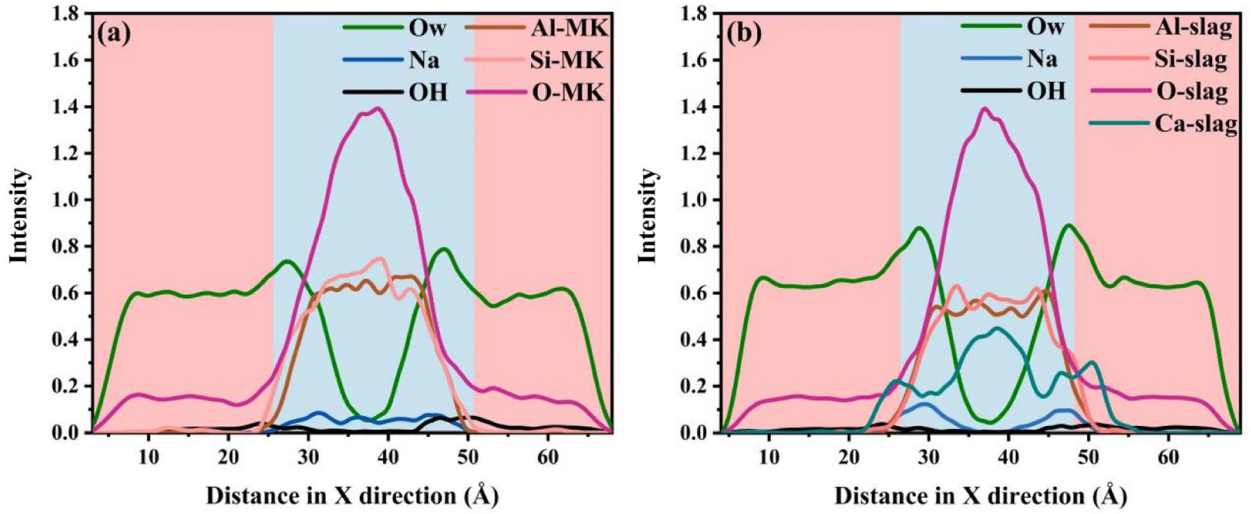

Fig. 4 (a) Atomic density distribution of metakaolin after activation; (b) atomic density distribution of slag after activation. Here, Na, OH, and Ow represent sodium ions, hydroxide ions, and oxygen atoms in water molecules of the NaOH solution respectively; Al-MK represents aluminum atoms in the metakaolin framework structure; the meanings of the other symbols are similar to the previous explanations.

the dissociation of the original slag structure. Notably, in contrast to the alkali-activated metakaolin system, in the alkali-activated slag system, Na^+ ions are merely adsorbed at the interface region without penetrating deeper positions. According to relevant ref. 43, the formation of a CASH gel phase is observed in the alkali-activated high-calcium system. The cationic component present in the interstitial spaces of the CASH gel framework is Ca^{2+}, which plays a role in maintaining charge balance and ensuring structural stability. In summary, during the alkali activation process, NaOH solution infiltrates into the minerals, causing dissociation and reformation of the crystal structure. However, the role of NaOH differs in the two systems. In the slag system, NaOH only serves as an activating agent and does not predominantly contribute to the formation of the new framework structure. On the other hand, in the metakaolin system, NaOH acts as both an activating agent and a major constituent of the newly formed framework structure. The dissolution process of ions is consistent with the observed reaction results mentioned earlier. Subsequently, a detailed analysis of the specific dissolution behavior of oligomers will be conducted.

3.2 Cluster dissolution process

Aluminosilicate oligomers are crucial reaction intermediates in the formation of NASH and CASH gels. In this section, we quantitatively analyze the formation status of aluminosilicate oligomers throughout the entire activation process. Q^n represents the connectivity state between silicate tetrahedra and Al–O polyhedra, which is used to characterize the formation of

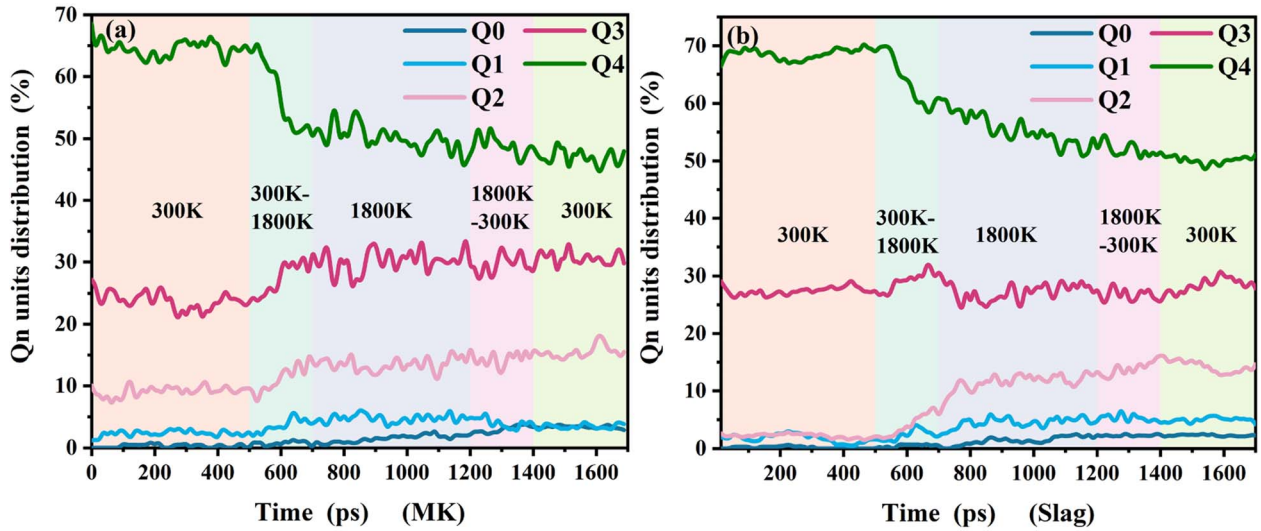

Fig. 5 (a) Evolution of the Q^n unit during dissolution of metakaolin; (b) evolution of the Q^n unit during dissolution of slag.

oligomers. As shown in Fig. 5, in the first stage (300 K), when there is no significant chemical reaction occurring yet, silicon and aluminum atoms in MK are present in the form of tetrahedra and octahedra, respectively, within a layered structure. In slag, most silicon and aluminum atoms are present in the form of tetrahedra within a layered structure, with a relatively high proportion of Q^4 and Q^3. As the temperature increases, the quantity of Q^4 decreases, while the number of Q^0 monomers, Q^1 dimers, and Q^2 short-chain structures significantly increases. This indicates the occurrence of deconstruction and leaching of mineral structures in the alkaline environment. Combined with Fig. 6, it is observed that monomers and dimers of silicate

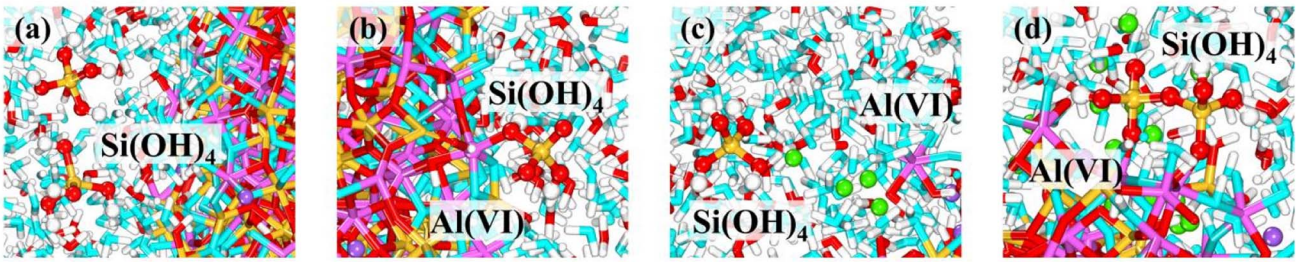

Fig. 6 (a) and (b) oligomers dissolved in MK system after alkali activation; (c) and (d) oligomers dissolved in slag system after alkali activation.

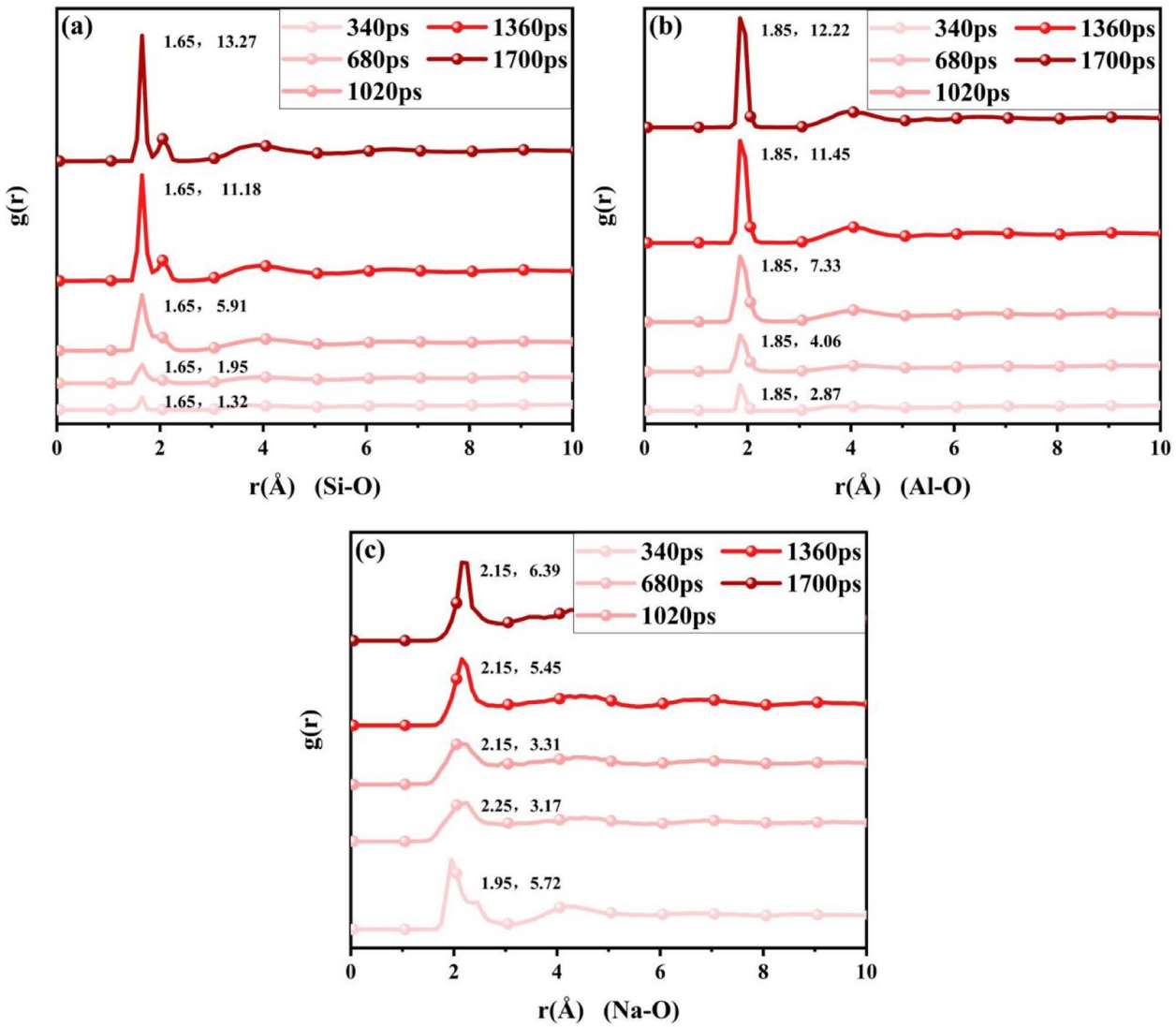

Fig. 7 Plot of radial distribution function at different time stages (MK system): (a) Si–O; (b) Al–O; (c) Na–O.

tetrahedra, among other oligomers, appear in the regions in contact with NaOH, which are important precursor materials for the formation of C(N)ASH gels. Additionally, the study also reveals that although some Q^4 deconstructs into oligomers, in the final stage at 300 K, Q^4 still occupies a significant proportion. This is because, in the late stages of the reaction, dissolved aluminosilicate oligomers aggregate into a reticular framework structure of C(N)ASH. Another reason is that the deconstruction phenomenon mainly occurs on the surfaces in direct contact with NaOH solution, while evident termination occurs in the interior. This also indicates that geopolymer mineral precursors can better deconstruct only when they come into sufficient contact with strong alkaline environments.

3.3 Bond length variations

The radial distribution function (RDF) plot is an important parameter for reflecting interatomic interactions. The horizontal axis of the curve represents the distance between two atoms in a chemical bond, while the vertical axis represents the probability of the two atoms being at different distances. Therefore, a higher value on the vertical axis indicates a greater concentration of chemical bonds at the corresponding distance. Fig. 7 illustrates the RDF plots of Si–O, Al–O, and Na–O bonds at various time stages in MK. Previous research indicates that the Si–O bond lengths are distributed within the range of 1.5–1.8 Å, Al–O bond lengths within the range of 1.7–2.1 Å, and Na–O bond lengths within the range of 2–3 Å.[44] The simulated bond lengths primarily fall within the range of 1.65 Å, 1.85 Å, and 1.95–2.25 Å, which is consistent with previous studies. Additionally, with the prolongation of alkali activation time, the peak intensities of Si–O and Al–O bonds increase, indicating an increasing number of oxygen atoms surrounding the silicon and aluminum atoms. More bridging oxygen atoms in the MK system undergo bond breaking and transform into non-bridging oxygen atoms, leading to the gradual dissociation and conversion of MK into oligomeric states. At 340 ps, the peak

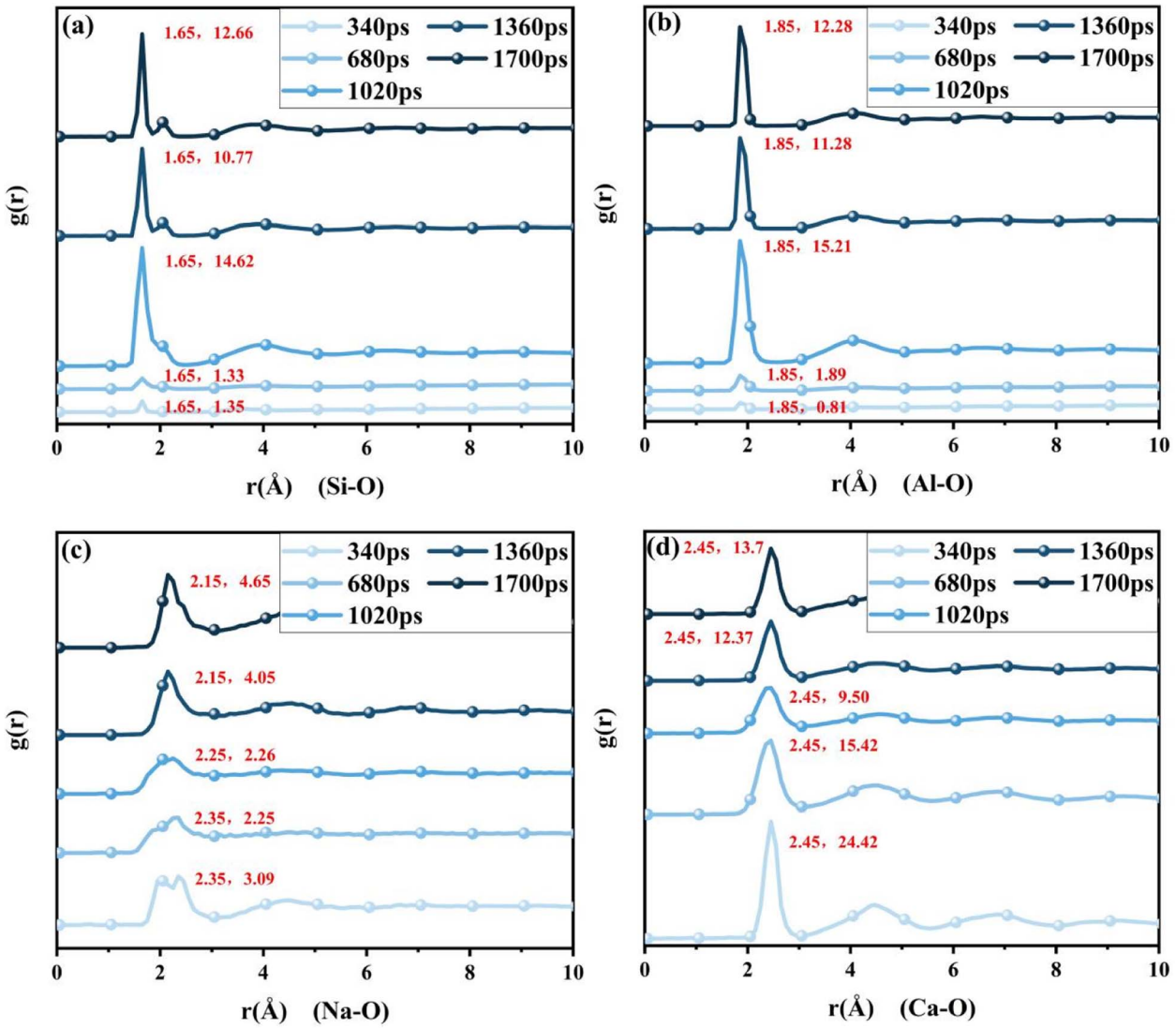

Fig. 8 Plot of radial distribution function at different time stages (slag system): (a) Si–O; (b) Al–O; (c) Na–O; (d) Ca–O.

intensity of Na–O is relatively high, indicating that most oxygen atoms bonded with Na^+ ions originate from the initial OH^- ions in the solution. At 680 ps and 1020 ps, the peak intensity weakens, suggesting that as MK dissolves, Na^+ ions gradually infiltrate into the interstitial spaces of the aluminosilicate framework. During this process, NaOH gradually disappears, and sodium primarily exists in the form of free Na^+ ions. Subsequently, at 1360 ps and 1700 ps, the peak intensities rise again, indicating that all Na^+ ions have entered the interior of MK and combined with the remaining aluminum and silicon atoms in the network through oxygen atoms.

Fig. 8 shows the RDF plots of Si–O, Al–O, Na–O, and Ca–O bonds at different time stages in slag. The bond lengths of Si–O, Al–O, and Na–O primarily fall within the ranges of 1.65 Å, 1.85 Å, and 2.15–2.35 Å, respectively, and their peak intensities are also within reasonable ranges. However, with the increase in alkali activation time, the peak intensities of Si–O and Al–O bonds gradually increase, reaching their maximum at 1020 ps. This indicates that in the high-calcium system, the atoms are more reactive, with lower energy barriers for chemical reactions, resulting in faster interatomic reaction rates and the occurrence of deconstruction phenomena in a shorter time. Subsequently, the peak intensities weaken, which can be attributed to the decrease in temperature in the later stages, leading to a reduction in atomic activity. Some of the deconstructed oligomers reassemble into polymerized states. The variation in peak intensity of Na–O bonds in different stages is similar to that in the MK system, but the peak intensities in each stage are significantly lower than those in the MK system. This is because Na^+ ions have not fully penetrated the interior of the slag and are not a major component of the CASH gel network structure. Inside the slag, Na^+ ions only exist at interface positions, where they are bound to a small number of oxygen atoms. On the other hand, in the high-calcium system, Ca^{2+} ions present in the slag play a role in charge balancing, filling the interstitial spaces in the aluminosilicate framework. This leads to the formation of

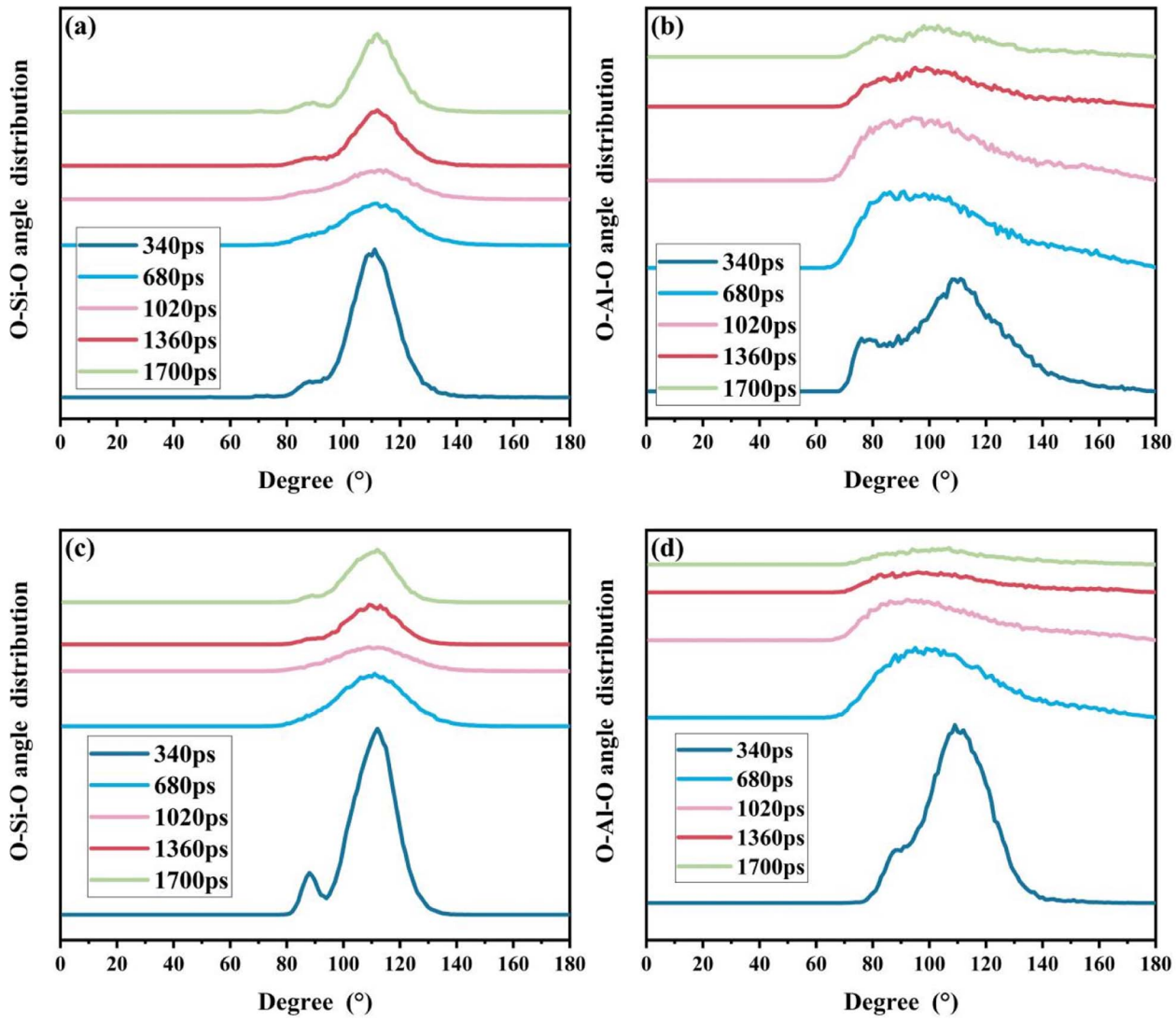

Fig. 9 Bond angle distribution function: (a) variation of bond angle of O–Si–O in MK system; (b) variation of bond angle of O–Al–O in MK system; (c) variation of bond angle of O–Si–O in slag system; (d) variation of bond angle of O–Al–O in slag system.

a high-calcium geopolymer gel phase, CASH, wherein Na^+ ions are not strongly attracted to the internal framework of the aluminosilicate. As a result, a strong Na–O peak is not formed. At 380 ps, a strong peak in Ca–O ionic bonds is formed. This peak is attributed to the stable presence of Ca in the matrix structure, where some Ca ions bind to external oxygen atoms, while others stably exist within the crystal structure of the slag, forming strong ionic coordination with oxygen in the silicate and aluminate tetrahedra. At 680 ps and 1020 ps, the peak intensity decreases. This is due to the intrusion of the strong alkaline solution into the mineral structure, leading to the disruption of connected aluminate and silicate tetrahedra, releasing Ca^{2+} ions in the form of free Ca ions. At 1360 ps and 1700 ps, the peak intensity increases again. The stimulated Ca ions are attracted by the aluminosilicate tetrahedra and form stable coordination, gradually forming the CASH gel phase. In summary, compared to the MK system, the slag is faster in its response to activation and the formation of the main geopolymeric gel phase.

3.4 Bond angle variations

Fig. 9 displays the evolution of bond angle distributions for O–Si–O and O–Al–O in both the MK and slag systems. According to the relevant ref. 45, the bond angle of O–Si–O is primarily distributed between 95° and 125°, with a peak near 109°. As shown in Fig. 9(a), because silicon in the MK system primarily exists in a tetrahedral form, uniformly and orderly in the mineral structure, a pronounced peak appears near 109° at 340 ps. As the reaction progresses, the peak intensity gradually decreases, and the angle range becomes wider, indicating the dissolution of more oligomers from MK. Compared to the layered and ordered arrangement in the solid phase of MK, at 1360 ps and 1700 ps, the peak intensity increases again, and the angle range narrows. This is because the dissolved oligomers polymerize, forming a reticular NASH structure where the silicate tetrahedra are once again fixed, resulting in the formation of an aluminosilicate framework. The bond angle distribution of O–Al–O ranges from 70° to 140°, much wider compared to the bond angle distribution of O–Si–O. This is due to the more complex forms of aluminum, including tetrahedral Al(IV), hexahedral Al(V), and octahedral Al(VI). As shown in Fig. 9(b), at 340 ps, two peaks appear at around 75° and 109° for O–Al–O. In the MK system, aluminum primarily exists in the forms of Al(IV) and Al(VI). As the reaction progresses, the peak intensities at 75° and 109° gradually decrease, while a peak gradually emerges at around 90°. This is because Al(IV) and Al(VI) have lower reactivity and dissolve into oligomers, existing in the form of Al(V). At 1360 ps and 1700 ps, two peaks reappear at 75° and 109°, indicating that aluminum recombines with the framework structure in the forms of tetrahedral and octahedral coordination, evolving into NASH gel.

Fig. 9(c) illustrates the evolution of O–Si–O bond angles in the slag system with reaction time. Similar to the MK system, silicon initially exists in a tetrahedral form. Subsequently, the peak intensity weakens as the silicate tetrahedra dissociates into oligomers. Then, the peak intensity increases as the silicate tetrahedra becomes fixed, and the gel gradually evolves into CASH gel. As shown in Fig. 9(d), at 340 ps, O–Al–O only exhibits a peak at 109°. This is because, in the slag, aluminum is primarily orderly and fixed in a tetrahedral form within the layered framework. As the activation reaction proceeds, the reactivity of the aluminate tetrahedra decreases, quickly transforming into a pentahedral structure. Therefore, at 680 ps and 1020 ps, the O–Al–O peak gradually emerges around 90°. Finally, the peak reappears at 109°, indicating that the Al–O pentahedral eventually transforms back into a tetrahedral structure and bridge within the framework structure.

4 Conclusion

This study investigates and simulates the initial reaction processes of metakaolin and slag in strong alkaline solutions to form low-calcium (NASH) and high-calcium (CASH) geopolymer cementitious materials from a molecular perspective. The study reveals the progression of geopolymer cementitious materials from mineral precursors to monomers, dimers, short-chain structures, and ultimately to amorphous complex structures. The main conclusions drawn from the research are as follows:

1. The formation of NASH and CASH involves two processes: firstly, the mineral precursors of metakaolin and slag undergo a deconstruction phenomenon in the NaOH alkaline environment, resulting in the formation of monomers, dimers, and short-chain structures as oligomers. Then, these oligomers undergo polymerization reactions, leading to the formation of amorphous, non-crystalline gel structures.

2. The role of NaOH differs slightly between the two systems. In the slag system, NaOH acts solely as an activator and does not constitute a major component of the new framework structure. However, in the metakaolin system, NaOH serves both as an activator and as a primary component of the new framework structure.

3. Compared to the low-calcium MK system, the atoms in the high-calcium slag system are more reactive, leading to faster deconstruction reactions and a greater propensity to form the main gel phase of geopolymer.

4. In the reaction processes of both systems, silicon atoms remain relatively stable, maintaining their silicate tetrahedral structures throughout. On the other hand, aluminum atoms are more reactive, experiencing changes in coordination structures and ultimately bridging into the gel structure as tetrahedral units (NASH and CASH) or octahedral units (NASH).

Conflicts of interest

There are no conflicts to declare.

Acknowledgements

Financial support from the National Key Research and Development Program of China under Grant 2022YFE0133800, National Natural science foundation of China under Grant U2006224, 52178221, Natural science foundation of Shandong Province under Grant ZR2022YQ55, Taishan Scholars of

Shandong Province under Grant tsqn.202306232 are gratefully acknowledged.

References

1 F. Zhang, X. Y. Wang and G. Liu, Allocation of carbon emission quotas based on global equality perspective, *Environ. Sci. Pollut. Res.*, 2022, **29**(35), 53553–53568, DOI: 10.1007/s11356-022-19619-8.

2 S. S. Dai, H. G. Wang, H. Wu and M. H. Zhang, Exploration of the mechanical properties, durability and application of geopolymers: a review, *Eur. J. Environ. Civ. Eng.*, 2023, **27**(10), 3202–3235, DOI: 10.1080/19648189.2022.2131633.

3 B. H. Jiang and M. Y. Raza, Research on China's renewable energy policies under the dual carbon goals: A political discourse analysis, *Energy Strateg. Rev.*, 2023, **48**, 10, DOI: 10.1016/j.esr.2023.101118.

4 E. Pawluczuk, K. Kalinowska-Wichrowska, J. R. Jiménez, J. M. Fernández-Rodríguez and D. Suescum-Morales, Geopolymer concrete with treated recycled aggregates: Macro and microstructural behavior, *J. Build. Eng.*, 2021, **44**, 15, DOI: 10.1016/j.jobe.2021.103317.

5 H. M. Tanu and S. Unnikrishnan, Mechanical Strength and Microstructure of GGBS-SCBA based Geopolymer Concrete, *J. Mater. Res. Technol.*, 2023, **24**, 7816–7831, DOI: 10.1016/j.jmrt.2023.05.051.

6 K. Zhang, H. Xu, X. X. Kong, C. Y. Zhang, H. F. Lu and D. He, Study on the influence mechanism of micro-mechanical properties of heterogeneous geopolymer gels, *J. Build. Eng.*, 2023, **76**, 11, DOI: 10.1016/j.jobe.2023.107164.

7 S. Dadsetan, H. Siad, M. Lachemi and M. Sahmaran, Extensive evaluation on the effect of glass powder on the rheology, strength, and microstructure of metakaolin-based geopolymer binders, *Constr. Build. Mater.*, 2021, **268**, 16, DOI: 10.1016/j.conbuildmat.2020.121168.

8 M. B. Ogundiran and S. Kumar, Synthesis and characterisation of geopolymer from Nigerian Clay, *Appl. Clay Sci.*, 2015, **108**, 173–181, DOI: 10.1016/j.clay.2015.02.022.

9 T. Phoo-Ngernkham, A. Maegawa, N. Mishima, S. Hatanaka and P. Chindaprasirt, Effects of sodium hydroxide and sodium silicate solutions on compressive and shear bond strengths of FA-GBFS geopolymer, *Constr. Build. Mater.*, 2015, **91**, 1–8, DOI: 10.1016/j.conbuildmat.2015.05.001.

10 M. Albitar, M. S. M. Ali and P. Visintin, Experimental study on fly ash and lead smelter slag-based geopolymer concrete columns, *Constr. Build. Mater.*, 2017, **141**, 104–112, DOI: 10.1016/j.conbuildmat.2017.03.014.

11 M. A. Gómez-Casero, C. De Dios-Arana, J. S. Bueno-Rodríguez, L. Pérez-Villarejo and D. Eliche-Quesada, Physical, mechanical and thermal properties of metakaolin-fly ash geopolymers, *Sustainable Chem. Pharm.*, 2022, **26**, 14, DOI: 10.1016/j.scp.2022.100620.

12 M. Catauro, V. Viola and A. D'Amore, Mosses on Geopolymers: Preliminary Durability Study and Chemical Characterization of Metakaolin-Based Geopolymers Filled with Wood Ash, *Polymers*, 2023, **15**(7), 17, DOI: 10.3390/polym15071639.

13 A. A. Siyal, M. R. Shamsuddin, M. I. Khan, N. E. Rabat, M. Zulfiqar, Z. Man, J. Siame and K. A. Azizli, A review on geopolymers as emerging materials for the adsorption of heavy metals and dyes, *J. Environ. Manage.*, 2018, **224**, 327–339, DOI: 10.1016/j.jenvman.2018.07.046.

14 S. Marathe, I. R. Mithanthaya and R. Y. Shenoy, Durability and microstructure studies on Slag-Fly Ash-Glass powder based alkali activated pavement quality concrete mixes, *Constr. Build. Mater.*, 2021, **287**, 18, DOI: 10.1016/j.conbuildmat.2021.123047.

15 N. A. Jaya, L. Yun-Ming, H. Cheng-Yong, M. M. A. Abdullah and K. Hussin, Correlation between pore structure, compressive strength and thermal conductivity of porous metakaolin geopolymer, *Constr. Build. Mater.*, 2020, **247**, 12, DOI: 10.1016/j.conbuildmat.2020.118641.

16 X. J. Wang, W. Yang, H. Liu, P. H. Zhu, N. W. Zong and J. C. Feng, Strength and Microstructural Analysis of Geopolymer Prepared with Recycled Geopolymer Powder, *J. Wuhan Univ. Technol., Mater. Sci. Ed.*, 2021, **36**(3), 439–445, DOI: 10.1007/s11595-021-2428-4.

17 N. H. Jamil, M. M. A. Abdullah, W. Ibrahim, R. Rahim, A. V. Sandu, P. Vizureanu, J. Castro-Gomes and J. M. Gómez-Soberón, Effect of Sintering Parameters on Microstructural Evolution of Low Sintered Geopolymer Based on Kaolin and Ground-Granulated Blast-Furnace Slag, *Crystals*, 2022, **12**(11), 11, DOI: 10.3390/cryst12111553.

18 N. H. Jamil, M. M. A. Abdullah, F. C. Pa, H. Mohamad, W. Ibrahim and J. Chaiprapa, Influences of SiO_2, Al_2O_3, CaO and MgO in phase transformation of sintered kaolin-ground granulated blast furnace slag geopolymer, *J. Mater. Res. Technol.*, 2020, **9**(6), 14922–14932, DOI: 10.1016/j.jmrt.2020.10.045.

19 M. Xia, H. S. Shi and X. L. Guo, Probing the structural evolution during the geopolymerization process at an early age using proton NMR spin-lattice relaxation, *Mater. Lett.*, 2014, **136**, 222–224, DOI: 10.1016/j.matlet.2014.08.022.

20 Q. Liu, Z. Y. Chen, Z. M. El-Bahy, P. Wang, S. N. Abdou, M. M. Ibrahim, Y. Wan, J. X. Wang, H. D. Li, L. Li and H. Wang, Alkali-hydrothermal activation of tailings with red mud as a supplementary alkali source to synthesize one-part geopolymer, *Adv. Compos. Hybrid Mater.*, 2023, **6**(4), 15, DOI: 10.1007/s42114-023-00707-3.

21 Q. Liu, M. Y. Cui, X. C. Li, J. X. Wang, Z. M. Wang, L. Li and X. J. Lyu, Alkali-hydrothermal activation of mine tailings to prepare one-part geopolymer: activation mechanism, workability, strength, and hydration reaction, *Ceram. Int.*, 2022, **48**(20), 30407–30417, DOI: 10.1016/j.ceramint.2022.06.318.

22 C. Ma, B. Zhao, L. M. Wang, G. C. Long and Y. J. Xie, Clean and low-alkalinity one-part geopolymeric cement: effects of sodium sulfate on microstructure and properties, *J. Cleaner Prod.*, 2020, **252**, 11, DOI: 10.1016/j.jclepro.2019.119279.

23 G. H. Gu, T. Ma, F. Chen, F. Xu and J. L. Zhang, Electromagnetic and mechanical properties of FA-GBFS

geopolymer composite used for induction heating of airport pavement, *Cem. Concr. Compos.*, 2022, **129**, 11, DOI: 10.1016/j.cemconcomp.2022.104503.

24 Z. N. Tian, Z. Q. Zhang, H. B. Liu, W. Z. Zheng, X. M. Tang and Z. J. Gui, Interfacial characteristics and mechanical behaviors of geopolymer binder with steel slag aggregate: insights from molecular dynamics, *J. Cleaner Prod.*, 2022, **362**, 13, DOI: 10.1016/j.jclepro.2022.132385.

25 R. Wang, J. S. Wang and Q. C. Song, The effect of Na^+ and H_2O on structural and mechanical properties of coal gangue-based geopolymer: molecular dynamics simulation and experimental study, *Constr. Build. Mater.*, 2021, **268**, 11, DOI: 10.1016/j.conbuildmat.2020.121081.

26 R. Wang, J. Y. Ye, J. S. Wang and X. Y. Peng, Adsorption and diffusion mechanism of cesium and chloride ions in channel of geopolymer with different Si/Al ratios: molecular dynamics simulation, *J. Radioanal. Nucl. Chem.*, 2023, **332**(9), 3597–3607, DOI: 10.1007/s10967-023-09046-5.

27 Q. Tang, M. Sun, X. Lu, D. Hou, M. Li and P. Wang, Understanding erosion resistance mechanisms of sodium aluminate silicate hydrate in erosion environments: a molecular dynamics study, *RSC Adv.*, 2024, **14**(15), 10397–10408, DOI: 10.1039/d4ra00302k.

28 B. Yin, T. H. Kang, J. T. Kang and Y. J. Chen, Analysis of Active Ion-Leaching Behavior and the Reaction Mechanism During Alkali Activation of Low-Calcium Fly Ash, *Int. J. Concr. Struct. Mater.*, 2018, **12**(1), 50, DOI: 10.1186/s40069-018-0282-3.

29 D. Hou, F. Hong, B. Dong, P. Wang, Y. Zhang, X. Wang and M. Wang, Molecular Insights into the Reaction Process of Alkali-Activated Metakaolin by Sodium Hydroxide, *Langmuir*, 2022, **38**(37), 11337–11345, DOI: 10.1021/acs.langmuir.2c01631.

30 X. Luo, X. Tian, J. Wu, X. Yang, Z. Liu, Z. Jiao and H. Peng, Molecular simulations of the initial stage's induction and formation process of N–A–S–H Gel based on NaOH-activated Metakaolin, *J. Non-Cryst. Solids*, 2024, **626**, 122804, DOI: 10.1016/j.jnoncrysol.2023.122804.

31 C. E. White, J. L. Provis, T. Proffen, D. P. Riley and J. S. J. van Deventer, Combining density functional theory (DFT) and pair distribution function (PDF) analysis to solve the structure of metastable materials: the case of metakaolin, *Phys. Chem. Chem. Phys.*, 2010, **12**(13), 3239–3245, DOI: 10.1039/b922993k.

32 A. Gualtieri and M. Bellotto, Modelling the structure of the metastable phases in the reaction sequence kaolinite-mullite by X-ray scattering experiments, *Phys. Chem. Miner.*, 1998, **25**(6), 442–452, DOI: 10.1007/s002690050134.

33 I. W. M. Brown, K. J. D. MacKenzie, M. E. Bowden and R. H. Meinhold, Outstanding Problems in the Kaolinite-Mullite Reaction Sequence Investigated by 29Si and 27Al Solid-state Nuclear Magnetic Resonance: 11, High-Temperature Transformations of Metakaolinite, *J. Am. Ceram. Soc.*, 1985, **68**, 298–301.

34 J. Lemaître, A. Léonard and B. Delmon, *Le mécanisme de la transformation thermique de la métakaolinite*, 1982.

35 N. Granizo, A. Palomo and A. Fernandez-Jiménez, Effect of temperature and alkaline concentration on metakaolin leaching kinetics, *Ceram. Int.*, 2014, **40**(7), 8975–8985, DOI: 10.1016/j.ceramint.2014.02.071.

36 X. D. Dai, S. Aydin, M. Y. Yardimci, K. Lesage and G. De Schutter, Early age reaction, rheological properties and pore solution chemistry of NaOH-activated slag mixtures, *Cem. Concr. Compos.*, 2022, **133**, 12, DOI: 10.1016/j.cemconcomp.2022.104715.

37 A. C. T. van Duin, A. Strachan, S. Stewman, Q. Zhang, X. Xu and W. A. Goddard, ReaxFFSiO Reactive Force Field for Silicon and Silicon Oxide Systems, *J. Phys. Chem. A*, 2003, **107**(19), 3803–3811, DOI: 10.1021/jp0276303.

38 D. S. Hou, C. Lu, T. J. Zhao, P. Zhang and Q. J. Ding, Structural, dynamic and mechanical evolution of water confined in the nanopores of disordered calcium silicate sheets, *Microfluid. Nanofluid.*, 2015, **19**(6), 1309–1323, DOI: 10.1007/s10404-015-1646-5.

39 D. S. Hou, T. J. Zhao, P. G. Wang, Z. J. Li and J. R. Zhang, Molecular dynamics study on the mode I fracture of calcium silicate hydrate under tensile loading, *Eng. Fract. Mech.*, 2014, **131**, 557–569, DOI: 10.1016/j.engfracmech.2014.09.011.

40 D. S. Hou, H. Y. Ma, Z. J. Li and Z. Q. Jin, Molecular simulation of "hydrolytic weakening": a case study on silica, *Acta Mater.*, 2014, **80**, 264–277, DOI: 10.1016/j.actamat.2014.07.059.

41 M. R. Sadat, K. Muralidharan and L. Y. Zhang, Reactive molecular dynamics simulation of the mechanical behavior of sodium aluminosilicate geopolymer and calcium silicate hydrate composites, *Comput. Mater. Sci.*, 2018, **150**, 500–509, DOI: 10.1016/j.commatsci.2018.04.041.

42 S. Plimpton, P. Crozier and A. Thompson, LAMMPS-large-scale atomic/molecular massively parallel simulator, *J. Appl. Phys.*, 2015, **118**(1), 14902.

43 D. Zhang, Z. J. Yang, D. Kang, C. Y. Fang, Y. Jiao, K. Y. Wang and S. Z. Mi, Study on the mechanism of Ca^{2+} and Na^+ interaction during the hydration of multi-source solid waste geopolymers, *J. Build. Eng.*, 2023, **69**, 14, DOI: 10.1016/j.jobe.2023.106177.

44 M. Zhang, N. A. Deskins, G. P. Zhang, R. T. Cygan and M. J. Tao, Modeling the Polymerization Process for Geopolymer Synthesis through Reactive Molecular Dynamics Simulations, *J. Phys. Chem. C*, 2018, **122**(12), 6760–6773, DOI: 10.1021/acs.jpcc.8b00697.

45 G. S. Henderson, D. R. Neuville, B. Cochain and L. Cormier, The structure of GeO_2–SiO_2 glasses and melts: a Raman spectroscopy study, *J. Non-Cryst. Solids*, 2009, **355**(8), 468–474, DOI: 10.1016/j.jnoncrysol.2009.01.024.